A Monte Carlo simulation of mode-locked hot-hole laser operation

1994 J. Phys.: Condens. Matter 6 7461

(http://iopscience.iop.org/0953-8984/6/36/025)

J. Phys.: Condens. Matter 6 (1994) 7461–7468. Printed in the UK

A Monte Carlo simulation of mode-locked hot-hole laser operation

R C Strijbos, J G S Lok and W Th Wenckebach
Delft University of Technology, Faculty of Applied Physics, PO Box 5046, 2600 GA Delft, The Netherlands

Received 24 March 1994

Abstract. We propose a method to achieve mode-locking in a p-germanium intervalenceband laser by modulating its gain. This is done by applying an additional radiofrequency (RF) electric field parallel to the applied magnetic field. Due to the acceleration by this RF field, the light holes are no longer accumulated in the so-called passive region below the optical phonon energy and the population inversion between the light and heavy hole band decreases strongly. A single-particle Monte Carlo simulation is used to study this effect more quantitatively. It is shown that an RF field of only a few per cent of the applied DC electric field already yields a peak-to-peak gain modulation of 30–50%. It is estimated that by using this method for actively mode-locking a p-Ge intervalenceband laser, picosecond FIR pulses of considerable power can be obtained.

In the past decade the p-germanium hot-hole laser has been proven to be a potential source of stimulated radiation in the far infrared wavelength range ($\lambda = 80$–$250\,\mu$m) [1]. By applying crossed $\boldsymbol{E}$ (≈ 0.3–$4\,\mathrm{kV\,cm^{-1}}$) and $\boldsymbol{B}$ (≈ 0.3–$4\,\mathrm{T}$) fields to a rectangular block of moderately p-doped germanium (N_A–$N_D \approx 10^{14}\,\mathrm{cm^{-3}}$) at helium temperature, laser action has been obtained in a frequency range of 40–$125\,\mathrm{cm^{-1}}$ with an output power up to a few watts. Two different types of laser action are known. The first involves population inversion between a pair of light hole Landau levels, while the other is based on a population inversion between the light and heavy hole band. This latter intervalenceband (IVB) laser has the interesting feature that it has a large quasi-homogeneous gain bandwidth, so it potentially supports mode-locked operation.

In this paper we consider an actively mode-locked IVB laser, where the gain of the laser is modulated at the cavity round-trip frequency by applying an RF electric field $\boldsymbol{E}'$ parallel to the magnetic field $\boldsymbol{B}$. Our modulation method is based on the observation of Shastin and co-workers, that the laser action of an IVB laser is completely destroyed upon changing the angle between $\boldsymbol{E}$ and $\boldsymbol{B}$ from 90° to 87° [2, 3]. In order to explain this effect, let us consider the pumping mechanism of the IVB laser as shown in figure 1, where the light and heavy hole subbands with effective masses $m_h = 0.35m_0$ and $m_l = 0.043m_0$ are shown, where m_0 is the free electron mass. At low temperatures, the scatter probability of holes with a kinetic energy ε less than the optical phonon energy ε_0 is determined by ionized impurity and acoustic phonon scattering only. For $\varepsilon > \varepsilon_0$ this probability is much higher due to strongly dominant optical phonon emissions. The gist of the p-germanium laser is that the strength of the applied crossed $\boldsymbol{E}$ and $\boldsymbol{B}$ fields are chosen such that the heavy and light holes behave in a different way: the light holes are 'trapped' in a region in $\boldsymbol{k}$-space where they do not reach ε_0, while the heavy holes are repetitively accelerated beyond ε_0 and scattered back by emitting an optical phonon (so-called streaming motion). Although most heavy holes are scattered back into the heavy hole band, about 4% is scattered into

0953-8984/94/367461+08$19.50

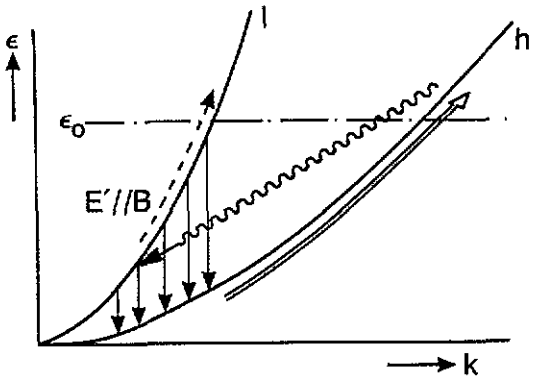

Figure 1. Pumping mechanism of an IVB laser. The light (l) and heavy (h) hole subbands are shown in energy–momentum space. The pumping cycle as described in the text is indicated. The broken line represents the acceleration of light holes up to ε_0 by the additional RF field $\boldsymbol{E}' \parallel \boldsymbol{B}$. After reaching ε_0 the light holes are predominantly scattered out of the accumulation region.

the light hole band. As a result a population inversion arises between the light and heavy hole band, which is used to achieve laser action.

However, the orthogonality of $\boldsymbol{E}$ and $\boldsymbol{B}$ is a critical parameter for population inversion. If $\boldsymbol{E}$ has a component along $\boldsymbol{B}$, the light holes are accelerated in the B direction (see the broken line in figure 1), and after they have reached the optical phonon energy ε_0 they are predominantly scattered out of the accumulation region. Thus the population inversion, and hence the gain of the IVB laser, is strongly reduced.

On account of these results, we expect that the small-signal gain can be strongly modulated with an RF electric field parallel to $\boldsymbol{B}$. However, the actual rise and decline of the population inversion is expected to depend critically on carrier dynamics. Therefore, we use Monte Carlo simulations to investigate the modulation of the laser gain due to an RF electric field parallel to $\boldsymbol{B}$. Finally, we estimate the pulse width of an actively mode-locked intervalenceband laser based on this principle.

Our Monte Carlo program simulates the propagation of holes in the light hole and heavy hole bands under the influence of crossed electric and magnetic fields in a similar way as in [4]. Here, only a short outline is given of the models used for the bandstructure and scatter mechanisms. A more detailed description is given elsewhere [5]. The anisotropy of the valence band is taken into account by using a parabolic 'warped' energy dispersion relation:

$$\epsilon_n(\boldsymbol{k}) = \frac{\hbar^2}{2m_0}[Ak^2 \pm g(\boldsymbol{k})] \tag{1}$$

with

$$g(\boldsymbol{k}) = [B^2k^4 + C^2(k_x^2k_y^2 + k_y^2k_z^2 + k_z^2k_x^2)]^{1/2} \tag{2}$$

with + and − for the light (n = l) and heavy (n = h) hole band respectively. Here $\hbar$ is the Planck constant, $\boldsymbol{k}$ is the reciprocal wavevector of the hole, and $A = 13.38$, $B = -8.48$ and $C = 13.14$ are the inverse valence band parameters of germanium. In our program all three types of carrier scattering that are involved in the pumping process, i.e. ionized impurity scattering, acoustic and non-polar optical phonon scattering, are incorporated, taking both intraband and interband scattering into account. Neutral impurity scattering is neglected since all carriers are ionized in the applied strong fields.

The total scatter rates for each process are expressed in simple analytic expressions by calculating them in the isotropic approximation. On the other hand, the anisotropy

is completely retained in the final state selection: a final state is selected according to its differential probability, using a standard rejection technique [6]. Here, optical phonon scattering, which is the dominant scatter process, has been implemented according to the deformation potential theory in the four-band model of Bir and Pikus [7, 8], including the quite complicated angular-dependent term. Acoustic phonon scattering is simplified in the usual way by using one effective acoustic deformation potential and the common overlap factors of Wiley [9]. We have included inelasticity, following the approach of [10, 11]. For ionized impurity scattering we used a modified form of the Brooks–Herring formulae of [10], implementing so-called statistical screening as proposed by Ridley [12, 13]. Details of the implementation of this model are given in [5].

In order to find the small-signal gain of the IVB laser, we calculate the (negative) absorption of radiation with a frequency ω due to the direct intersubband transition and its absorption due to indirect (intersubband and intrasubband) transitions, assisted by phonons or ionized impurities. The absorption cross section due to the direct IVB transition is given by

$$\sigma_{\mathrm{lh}} = \frac{\pi e^2 \hbar}{2m_0 \epsilon_0 \sqrt{\epsilon_r} c} \int \frac{2\mathrm{d}k}{(2\pi)^3} |\zeta_{\mathrm{lh}}(k)| [f_{\mathrm{h}}(k) - f_{\mathrm{l}}(k)] \delta[\varepsilon_{\mathrm{l}}(k) - \varepsilon_{\mathrm{h}}(k) - \hbar\omega] \tag{3}$$

where e is the electron charge, ε_0 the permittivity of the vacuum, ε_r the relative dielectric constant of the semiconductor, and c the velocity of light. The heavy and light hole distribution functions, denoted by f_{h} and f_{l} respectively, are normalized by

$$\int \frac{2\mathrm{d}k}{(2\pi)^3} [f_{\mathrm{l}}(k) + f_{\mathrm{h}}(k)] = 1 \tag{4}$$

and $\zeta_{\mathrm{lh}}(k)$ is the oscillator strength, which for non-polarized radiation is given by [14]

$$|\zeta_{\mathrm{lh}}(k)| = \left| A - \frac{m_0}{3\hbar^2} \sum_{i=x,y,z} \frac{\partial^2 \varepsilon(k)}{\partial k_i^2} \right|. \tag{5}$$

To derive the absorption due to indirect transitions, we have to use second-order time-dependent perturbation theory. The total absorption cross section due to indirect transitions becomes [4]

$$\sigma_{\mathrm{D}} = \frac{2\hbar^2}{c\epsilon_0 \sqrt{\epsilon_r} A_0^2 \hbar\omega} \int \frac{2\mathrm{d}k}{(2\pi)^3} \sum_{s,n,n'} \left[P_{nn'}^{s,\mathrm{a}}(k) - P_{nn'}^{s,\mathrm{e}}(k) \right] f_n(k) \tag{6}$$

with A_0 the amplitude of the vector potential of the radiation, and s an index denoting the scatter process; $\sum_{n'} P_{nn'}^{s,m}$ is the total indirect transition probability from an initial state nk to all possible final states $n'k'$ due to absorption ($m = \mathrm{a}$) or emission ($m = \mathrm{e}$) of a photon with energy $\hbar\omega$, assisted by scatter process s and

$$P_{nn'}^{s,m}(k) = \frac{V}{(2\pi)^3} \int \mathrm{d}k' \frac{2\pi}{\hbar} |M^s(k, k')|^2 \delta[\varepsilon_n(k) - \varepsilon_{n'}(k') \mp \hbar\omega \mp \varepsilon_q] \tag{7}$$

where $\mp\hbar\omega$ in the argument of the delta function corresponds to photon emission if the $+$ sign is chosen and photon absorption otherwise. The term $\mp\varepsilon_q$ only applies in the case of phonon-assisted scattering. Now the $-$ sign corresponds to emission and the $+$ sign to

absorption of a phonon with energy ε_q. Using an isotropic dispersion relation the matrix elements in (7) become

$$|M^s(k,k')|^2 = |H^s_{nn'}(k,k')|^2\left(\frac{eA_0\hbar}{2\hbar\omega}\right)^2\left(\frac{\hat{e}_\omega\cdot k}{m_n}-\frac{\hat{e}_\omega\cdot k'}{m_{n'}}\right)^2. \tag{8}$$

Here m_n is the density of states effective mass of subband n and $\hat{e}_\omega$ the unit polarization vector of the radiation; $|H^s_{nn'}(k,k')|^2$ is the squared transition matrix element for scatter process s, including the usual overlap factor. Simple isotropic models for these matrix elements yield analytic expressions for the twenty different indirect processes, as were obtained in [15]†. The integrals in both cross sections, given by (3) and (6), are evaluated by sampling the oscillator strength $|\zeta_{lh}(k)|$ or the transition probabilities $P^{s,m}_{nn'}$ directly during the Monte Carlo simulation. A typical result is shown in figure 2, where σ_{lh}, σ_D and the total absorption cross section $\sigma_{tot} = \sigma_{lh}+\sigma_D$ are evaluated as a function of the photon energy $\hbar\omega$. This simulation as well as those below are performed for non-polarized radiation and for a temperature $T = 10\,K$, an acceptor concentration $N_A = 2\times10^{14}\,cm^{-3}$, a donor concentration $N_D = 0$, an electric field $E = 2\,kV\,cm^{-1}$ along the [111] direction, and a magnetic field $B = 1.3\,T$ along the $[0\bar{1}1]$ direction. Figure 2 shows that the total absorption cross section is negative for $\hbar\omega = 4\,meV$ to $\hbar\omega = 32\,meV$, and thus FIR amplification can take place in this region with a maximum amplification coefficient $g_0 = -\sigma_{tot}(N_A - N_D) \approx 0.4\,cm^{-1}$ for $\hbar\omega = 11\,meV$.

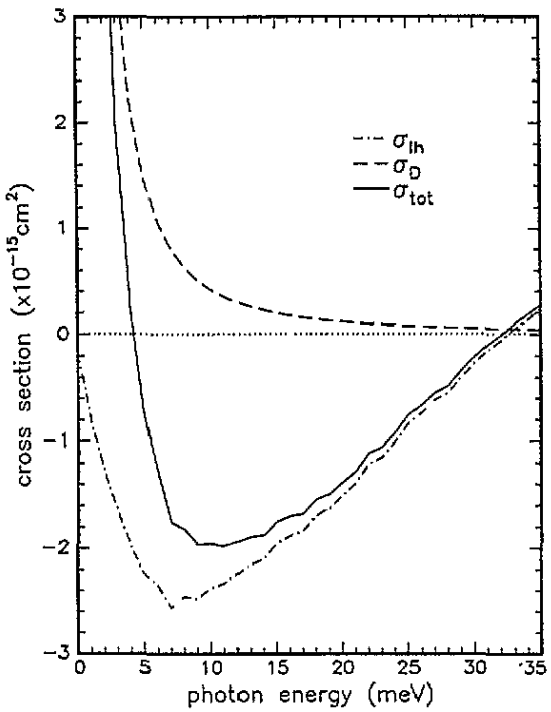

Figure 2. Absorption cross sections σ_{lh} of the direct transition, σ_D of the indirect transitions and the total absorption cross section $\sigma_{tot} = \sigma_{lh} + \sigma_D$ as a function of the photon energy $\hbar\omega$ for non-polarized radiation. $T = 10\,K$, $N_A = 2\times10^{14}\,cm^{-3}$, $N_D = 0$, $E = 2\,kV\,cm^{-1} \parallel [111]$, $B = 1.3\,T \parallel [0\bar{1}1]$.

† However, formulae (A6) and (A7) for ionized impurity-assisted indirect absorption have to be multiplied with a factor 1/2 and the last term in formula (A7), starting with $3k_fk_0$, should have a minus sign instead of a plus sign.

In order to investigate the influence of an additional RF electric field with angular frequency $\Omega = 2\pi f$, we use two methods, which were introduced by Lebwohl [16] for Monte Carlo simulations of transport properties. In both methods a single-particle Monte Carlo simulation is performed for many cycles of the RF field. In the first method, the period of the RF field is divided into a number of phase intervals and the response over one period is found by averaging the values of $A(t)$ sampled in each phase interval. The other method is based on a Fourier sine and cosine decomposition of the observable $A(t)$:

$$\langle A(t)\rangle = A_0 + \sum_{m=1}^{M}[A_m \sin(m\Omega t) + B_m \cos(m\Omega t)] \tag{9}$$

and the response is found by sampling the coefficients A_m and B_m, given by the inverse transformations

$$A_0 = N^{-1}\sum_{j=1}^{N} A(t_j) \tag{10}$$

$$A_m = 2N^{-1}\sum_{j=1}^{N} A(t_j)\sin(m\Omega t_j) \tag{11}$$

$$B_m = 2N^{-1}\sum_{j=1}^{N} A(t_j)\cos(m\Omega t_j) \tag{12}$$

where N is the total number of samples and the t_j correspond to the times at which the jth scattering occurs and $A(t)$ is sampled, using a synchronous ensemble [6]. The latter method can be much faster but this advantage vanishes in our case where, due to the non-linear response, Fourier coefficients of higher order also have to be taken into account. We find that by sampling the coefficients up to $M = 8$ the responses are identical for the two methods.

The results of the Monte Carlo calculations are shown in figure 3. The conditions are equal to that of figure 2, but now an additional RF electric field parallel to B is applied with frequency $f = 500\,\text{MHz}$. The main figure shows the response of σ_{lh} to the RF electric field, where the amplitude of the RF field is only 2% of the applied DC electric field or only $40\,\text{V cm}^{-1}$. It is observed that σ_{lh} is modulated considerably at the second harmonic of the RF frequency f and $-\sigma_{lh}$ passes through a maximum every 1.0 ns when the RF electric field is zero. It is also clear that the response is non-linear: σ_{lh} is more 'peaked' than the sinusoidal second harmonic of the applied perturbation. This is due to the fact that the population inversion is destroyed as soon as most light holes reach the threshold energy ε_0 in half a cycle of the RF field and are scattered out of the accumulation region. In the inset of figure 3 the peak-to-peak gain modulation depth has been calculated as a function of the amplitude of the perturbing RF field. From this picture it can be concluded that already small RF fields with an amplitude of only a few percent of the applied electric field are sufficient to obtain peak-to-peak modulation depths of more than 50%.

If we want to use this method of gain modulation to achieve an actively mode-locked p-Ge IVB laser, the small signal gain has to be modulated at the cavity round-trip frequency f_c. Taking into account that the small signal gain is modulated at the second harmonic of the RF electric field frequency, f has to be chosen equal to half the cavity round-trip time f_c. For example, in order to achieve mode-locking in a typical p-Ge IVB laser, consisting

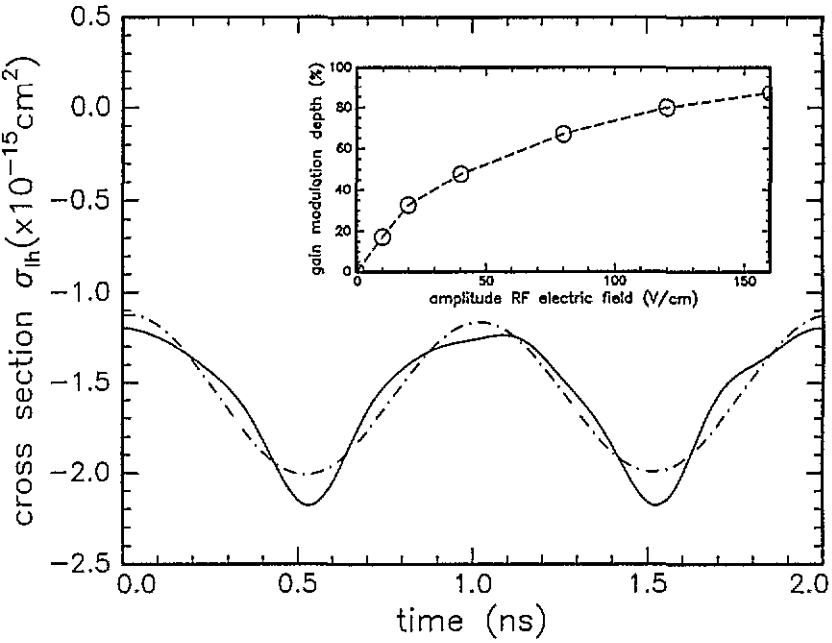

Figure 3. Absorption cross section for the direct IVB transition during one (cosine) period of the RF field, as calculated from (9) up to $M = 8$ (full curve) and $M = 2$ (chain curve). The amplitude of the RF field is only $40\,\mathrm{V\,cm^{-1}}$, so only 2% of the applied DC electric field; σ_{lh} is modulated considerably at the second harmonic of the RF frequency $f = 500\,\mathrm{MHz}$, but σ_{lh} is more 'peaked' than the second harmonic. The inset shows the peak-to-peak gain modulation depth as a function of the amplitude of the RF electric field, demonstrating that already small RF fields are sufficient to obtain peak-to-peak modulation depths of more than 50%.

of a germanium crystal of 37.5 mm with an external standing-wave resonator around it, an RF electric field with $f = 500\,\mathrm{MHz}$ has to be used.

In the time-domain picture of active mode locking, the gain modulation effectuates that only a short circulating pulse is sustained in the cavity. This pulse, passing through the active medium at the moment of maximum gain, will be shortened each round trip and become much shorter than the modulation period. This is illustrated in figure 4, where the normalized 'effective' gain after one and after a hundred round trips are shown. Since in a typical experimental laser set-up, it already takes a few hundred round trips to reach saturation in quasi-CW operation [18, 19], we can neglect effects of saturation for a hundred round trips. Therefore, it can be concluded that the pulse width after a hundred round trips is approximately 80 ps.

Finally we estimate the lowest possible width of output pulses that can be reached after a still larger number of round trips, when the spectral width of the pulse approaches the amplification bandwidth of the laser medium. For a laser based on a purely inhomogeneously broadened transition, the resulting steady-state pulse width $\tau_{p,ss}$ is determined by the inhomogeneous linewidth of the transition [17]:

$$\tau_{p,ss}^{inh} \approx \frac{0.5}{(\Delta f)_{inh}}. \tag{13}$$

For the IVB laser $\Delta f \approx 3\,\mathrm{THz}$ [18], so we would find an extremely short minimum pulse length $\tau_{p,ss}^{inh}$ corresponding to about one optical cycle.

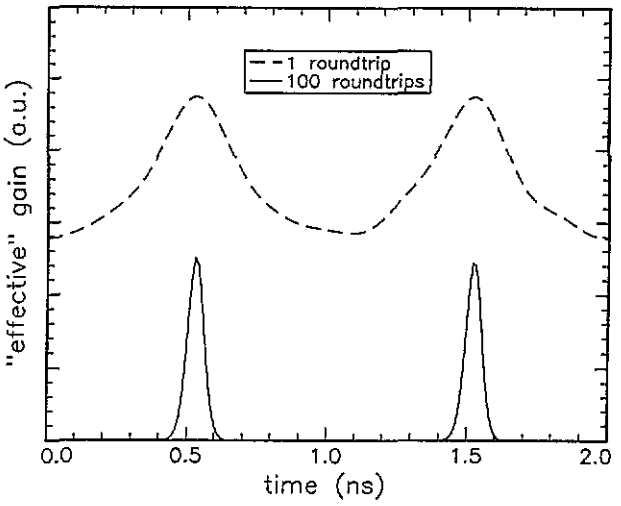

Figure 4. Normalized 'effective' gain after one and a hundred round trips, demonstrating the pulse-shortening effect.

However, $\tau_{p,ss}$ may be much larger, if a laser is based on a homogeneously broadened transition. In this case, the laser oscillates naturally only at one (or a few) axial modes just at line centre and the modulator has to generate additional sidebands to spread out the laser spectrum across the homogeneously broadened line [17]. Thus the steady-state pulse width $\tau_{p,ss}$ for an amplitude-modulated homogeneously broadened laser is given by

$$\tau_{p,ss}^{hom} \approx \frac{0.5}{[f_m(\Delta f)_{hom}]^{1/2}} \tag{14}$$

where f_m is the modulation frequency and $(\Delta f)_{hom}$ is the linewidth of the homogeneously broadened transition. If we now insert typical values ($f_m = 1\,GHz$ and $\Delta f_{hom} \approx 3\,THz$) in (14), we find $\tau_{p,ss}^{hom} = 9\,ps$.

In order to determine the character of the IVB transition, extensive saturation studies have been performed by Keilmann and co-workers, for both the passive (i.e. no applied fields) and the active p-type germanium under crossed electric and magnetic fields [18–20]. They concluded that although in the passive material the heavy–light hole transition is well described using a model of inhomogeneously broadened two-level systems ($\delta\nu_{inh} \approx 200\,cm^{-1}$, $\delta\nu_{hom} \approx 7\,cm^{-1}$), the active material is dominantly homogeneously broadened. This result is ascribed to the rapid carrier motion: the holes move very fast through the volume in energy–momentum space that is in resonance with the far infrared radiation, giving rise to homogeneous broadening which is expected to cover the full laser gain bandwidth [20]. Another factor of importance can be the broadening due to a small non-orthogonality of $\boldsymbol{E}$ and $\boldsymbol{B}$, as mentioned in [3].

Therefore the IVB transition may be largely homogeneously broadened and the steady-state pulse length will be $\tau_{p,ss}^{hom} = 9\,ps$ rather than $\tau_{p,ss}^{inh} = 0.2\,ps$. Furthermore, we note that in an actual experiment it may be difficult to have the laser oscillate stably 10^3–10^4 round trips before laser saturation, which is necessary for τ_p to decrease to its steady-state value $\tau_{p,ss}$.

Still, we may conclude that an actively mode-locked IVB laser, as proposed in this paper, may yield very short far infrared pulses in the order of 10–100 ps, that have thus far only been reached in free electron lasers [21].

Acknowledgments

The authors wish to thank S I Schets and J E Dijkstra for their contributions to the Monte Carlo program. This investigation is part of the research program of the 'Stichting voor Fundamenteel Onderzoek der Materie (FOM)' which is financially supported by the 'Nederlandse Organisatie voor Wetenschappelijk Onderzoek (NWO)'.

References

[1] Special issue 1991 *Opt. Quantum Electron.* **23**
[2] Shastin V N 1991 *Opt. Quantum Electron.* **23** S111
[3] Murav'ev A V, Nefedov I M, Pavlov S G and Shastin V N 1993 *Quantum Electron.* **23** 119
[4] Starikov E V and Shiktorov P N 1991 *Opt. Quantum Electron.* **23** S177
[5] Strijbos R C, Dijkstra J E, Schets S I and Wenckebach W Th 1994 to be published
[6] Jacoboni C and Reggiani L 1983 *Rev. Mod. Phys.* **55** 645
[7] Bir G L and Pikus G E 1974 *Symmetry and Strain-Induced Effects in Semiconductors* (New York: Wiley)
[8] Lawaetz P 1968 *Phys. Rev.* **174** 867
[9] Wiley J D 1971 *Phys. Rev.* B **4** 2485
[10] Brudevoll T, Fjeldly T A, Baek J, and Shur M S 1990 *J. Appl. Phys.* **67** 7373
[11] Jensen G U, Lund B, Fjeldly T A and Shur M S 1991 *Comput. Phys. Commun.* **67** 1
[12] Ridley B K 1977 *J. Phys. C: Solid State Phys.* **10** 1589
[13] Van de Roer T G and Widdershoven F P 1985 *J. Appl. Phys.* **59** 813
[14] Rebane Yu T 1983 *Sov. Phys. Solid State* **25** 1094
[15] Pozela J K, Starikov E V and Shiktorov P N 1985 *Litovsk. Fiz. Sborn.* **23** 7
[16] Lebwohl P A 1973 *J. Appl. Phys.* **44** 1744
[17] Siegman A E 1986 *Lasers* (Mill Valley: University Science Books)
[18] Keilman F and Till R 1991 *Opt. Quantum Electron.* **23** S231
[19] Keilman F, Shastin V N and Till R 1991 *Appl. Phys. Lett.* **58** 2205
[20] Keilman F and Till R 1992 *Semicond. Sci. Technol.* **7** B633
[21] Bakker R J, van der Geer C A J, Jaroszynski D A, van der Meer A F G, Oepts D, van Amersfoort P W, Anderegg V and van Son P C 1993 *Nucl. Instrum. Meth.* A **331** 79